Path integral calculation for asymmetric double-well potential: cumulant, Debye−Waller factor and chemical reaction

Takafumi Miyanaga, Kiyofumi Nitta

Department of Materials Science and Technology, Faculty of Science and Technology, Hirosaki University, Hirosaki, Aomori 036-8561, Japan

Takashi Fujikawa

Graduate School of Science, Chiba University, Yayoi-cho 1-33, Inage, Chiba, 263-8522, Japan

Path integral effective potential method is applied to symmetric and asymmetric double-well potential systems. We calculate the temperature dependence of 2nd, 3rd and 4th order cumulants, which are useful to study vibrational effects in various spectroscopic techniques. We evaluate the Debye–Waller factors in EXAFS, EELFS and XPD and discuss the characteristic features caused by asymmetric double-well potential. We also relate this method to the quantum tunneling effect in the simple chemical reaction rate constant.

PACS: 61.10.Ht
Key words: path integral, Debye–Waller factor, EXAFS, double-well potential

1 Introduction

X-ray, neutron, electron and γ-ray are useful direct probes for the structural analyses in condensed systems. At finite temperature, the thermal factors are important parameters to improve the accuracy in the structure determination and to reveal the structural dynamics of the system. Thermal factors in core spectroscopies such as Extended X-ray absorption fine structure (EXAFS), Electron energy loss spectra (EELS), and X-ray photoelectron diffraction (XPD) are important to study local atomic structures around an excited atom where interference effects of excited photoelectrons are used to obtain the structural information. They also provide useful information about atomic vibrations.

Theoretical aspects of temperature dependence of EXAFS were first studied [1] within the framework of harmonic vibration for nuclei motion and plane wave approximation for photoelectron waves. Since that time some improvements have been found beyond the harmonic approximation [2–5] and the plane wave approximation [6, 7]. When they include the anharmonic effects in EXAFS analyses, perturbation theory has been applied by use of temperature Green's function [3] or thermal perturbation theory [8]. These perturbation approaches are useful to describe weak anharmonicity in the analyses of temperature effects in EXAFS, EELS, XPD spectra, and they have provided interesting information based on cumulant expansion.

On the other hand real space approach [9] has been used to relate the EXAFS

thermal factors to interatomic potential, where the classical approximation is used. This approach can be safely used in high temperature region even though the anharmonicity is strong.

We have discussed a real space approach to study EXAFS thermal factor based on the finite temperature path-integral method originally developed by Feynman [10], later improved by Cuccoli et al. [11] and Feynman and Kleinert [12]. This self-consistent approach can be applied to strongly anharmonic systems and can be closely related to the classical formulas. We have studied the range of the applicability of widely used cumulant analysis and of the classical approximation for the EXAFS thermal factors [13–15]. These effective potential method by Yokoyama [16] and Path-Integral Monte Carlo (PIMC) method by Fornasini and coworkers [17] have been applied to EXAFS thermal analysis.

In this paper we apply the path integral effective potential method to one-dimentional symmetric and asymmetric double-well potential systems in a reservoir at temperature T. In $PbTiO_3$, atomic pair distribution function is well approximated by double-well potential and it shows "soft mode" behavior. Doll et al. studied some thermodynamical properties of small clusters by use of Fourier Path Integral analyses [18], in which atomic distribution function is also considered as asymmetric double-well potential. In the filled skutterudites, $PrOs_4Sb_{12}$ is known as 4f heavy fermion superconductor and shows an interesting rattling behavior suggested by ultrasonic measurement [19] in which Pr ion is considered to be moving in the double-well potential in the cage of Sb_{12}. We evaluate the cumulants, Debye–Waller factor and thermal dumping function in EXAFS for the model systems. This approach can be easily applicable to study the thermal factors in other spectroscopic methods as XRD, neutron diffraction, XPD, EELS and Mössbauer spectroscopy.

Such an asymmetric double-well potential can be considered as a chemical reaction models [20]. By use of the present path integral effective potential method [21, 22], we can calculate quantum tunneling correction to the simple unimolecule chemical reaction path.

2 Theory

Here we show the outline of the theory for later discussion. Details are shown in ref. [13]. Let consider diatomic systems in a reservoir whose relative vibrational motion is described by the Hamiltonian,

$$H = \frac{p^2}{2\mu} + V(q)\,, \tag{1}$$

where μ is the reduced mass and q is the instantaneous interatomic distance. When we deal with statistical average of an operator A, we should calculate the trace as in eq. (2),

$$\langle A \rangle = \frac{1}{Z}\ \mathrm{Tr}(A\rho)\,, \tag{2}$$

where ρ is the density operator defined by $\rho = \exp(-\beta H)$, $\beta = 1/k_{\rm B}T$ and $Z = \exp(-\beta F) = {\rm Tr}(\rho)$ is the partition function for the systems. The trace can be calculated by applying Feynman's path-integral techniques, however, instead of summing over all paths in just one step, one can classify the paths into two groups as proposed by Feynman [10]. One group consists of average (quasi classical) path $\bar{q}$ given by

$$\bar{q} = \frac{1}{\beta}\int_0^\beta q(u){\rm d}u\,, \quad \hbar = 1 \tag{3}$$

and the other group consists of quantum fluctuation around $\bar{q}$. The average path is the same as the classical path in the high temperature limit ($\beta \to 0$). To use the non-perturbation method based on the path-integral techniques, we approximate the instantaneous potential $V(q(u))$ by a trial potential quadratic in the fluctuation path $q - \bar{q}$, [10, 11],

$$V \cong V_0(q,\bar{q}) = w(\bar{q}) + \frac{\mu\omega(\bar{q})^2}{2}\,(q-\bar{q})^2\,. \tag{4}$$

Now the parameter $w(\bar{q})$ and $\omega(\bar{q})$ are to be optimized so that the trial reduced density $P(q)$ well approximate the true reduced density. A variational approach which gives the same result as the self-consistent approximation is also possible [10, 11]. Final expression for the average of a local operaor A can be represented in terms of the probability density $P(q)$ just like a classical statistical mecanichs (from now on q is used instead of $\bar{q}$ for brevity),

$$\langle A\rangle = \int A(q)P(q){\rm d}q\,. \tag{5}$$

This expression, however, includes important quantum effects, and the probability is represented by

$$P(q) = \frac{1}{Z}\sqrt{\frac{\mu}{2\pi\beta}}\,\exp\bigl[-\beta V_L(q)\bigr]\,, \tag{6}$$

where local effective potential $V_L(q)$ is defined by

$$\exp\left[-V_L(q)\right] = \int {\rm d}\xi \exp\bigl[-V_e(q+\xi)\bigr]\,\frac{1}{\sqrt{2\pi\alpha(q+\xi)}}\,\exp\left[-\frac{\xi^2}{2\alpha(q+\xi)}\right]. \tag{7}$$

Now we have used the relations

$$\begin{aligned}
\frac{V_e(q)}{\varepsilon} &= w(q) + \frac{1}{\beta}\,\ln\left(\frac{\sinh f(q)}{f(q)}\right), \\
f(q) &= \frac{\beta\omega(q)}{2}\,, \\
\alpha(q) &= \frac{1}{2\mu\omega(q)}\left(\coth f(q) - \frac{1}{f(q)}\right),
\end{aligned} \tag{8}$$

where ε is the energy scale. The local effective potential $V_L(q)$ is reduced to the bare potential $V(q)$ in the high temperature limit.

In the EXAFS analyses the operator A should be $\exp(2\mathrm{i}k\Delta_\alpha)$ where k is the wave vector of ejected photoelectrons ($k = |\mathbf{k}|$), and Δ_α is the projected relative displacement, which is simply given by $\Delta_\alpha = \Delta q = q - q_0$ in one-dimentional cases; q_0 is the equilibrium interatomic distance. So that what we should calculate to study EXAFS thermal factor is the thermal average including quantum fluctuation given by

$$\left\langle \exp(2\mathrm{i}k\Delta q) \right\rangle = \frac{1}{Z}\sqrt{\frac{\mu}{2\pi\beta}} \int \exp(2\mathrm{i}k\Delta q)\exp[-\beta V_L]\mathrm{d}q\,. \tag{9}$$

Any order of moments $\langle q^n \rangle$ is also calculated by use of the local effective potential $V_L(q)$

$$\langle q^n \rangle = \frac{1}{Z}\sqrt{\frac{\mu}{2\pi\beta}} \int q^n \exp[-\beta V_L(q)]\mathrm{d}q\,. \tag{10}$$

We now shifted the origin for the potential $V(q)$ to be $q_0 = 0$. This expression shows that the widely used real space representation is obtained with some modification from the quantum fluctuation effects: the original interatomic potential $V(q)$ should be replaced by the local effective potential $V_L(q)$ which is temperature dependent and tends to be $V(q)$ at high temperature from physical consideration. Though the discussion is only shown for the EXAFS thermal factors here, extension to EELS and XPD thermal factors is straightforward [13].

3 Results and discussion

In this section the method described in the previous section is applied to anharmonic diatomic systems in double-well potentials given by

$$\frac{V(q)}{\varepsilon} = (q^2 - \sigma^2)^2 + c\sigma\left(\frac{q^3}{3} - \sigma^2 q\right), \tag{11}$$

where σ is the minima of the potential well and c is the measure of asymmetry of the double-well potential: The strongly asymmetric potential is obtained for the large c. This potential has the absolute minimum at $q = \pm\sigma$ irrespective of c. We introduce a parameter g defined by

$$g = \sqrt{\frac{\hbar^2 v''\left(q_{\min}\right)}{\mu\varepsilon\sigma^2}}\,. \tag{12}$$

Small (large) g value gives rise to a weak (strong) quantum effect. By use of this parameter g, we define a reduced temperature t by

$$t = \left(\frac{\hbar^2 v''(q_{\min})}{\mu g \sigma^2 k_{\mathrm{B}}}\right)^{-1} T\,. \tag{13}$$

In the present paper we use energy scale ε and length scale σ for Cu-O in high-temperature superconductor $YBa_2Cu_3O_{7-\delta}$, [23, 24], which is a model for double-well potential. Figure 1 shows the double-well potential for various c values for $\sigma = 0.1\,\text{Å}$. By use of the self-consistent method described in section 2, we obtain $f(q)$ as a function of q from which we calculate $V_e(q)$ and $P(q)$.

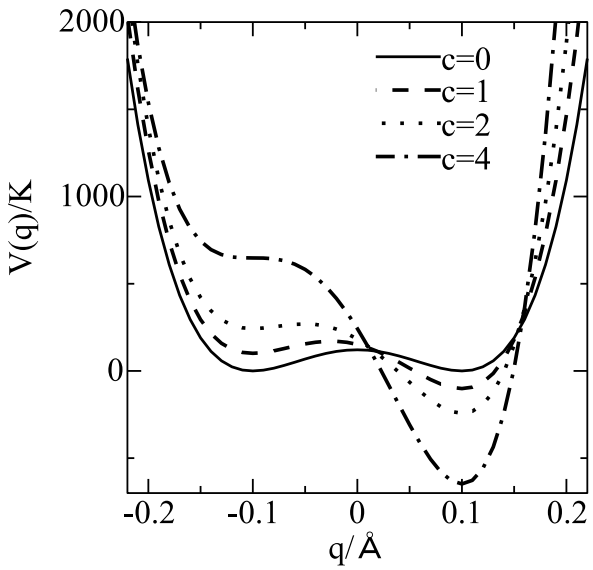

Fig. 1. The double-well potential $V(q)/\varepsilon = (q^2 - \sigma^2)^2 + \frac{1}{3}\, c\sigma q^3 - \sigma^2 q$, $c = 0,\ 1,\ 2,\ 4$. $\sigma = 0.1\,\text{Å}$ and $g = 5.0$.

3.1 Temperature dependence of cumulants in EXAFS thermal factor

From eq. (7) and (10) we can evaluate the second, third, and forth order cumulants $\langle \dots \rangle_c$ by use of the same and lower order moments,

$$\begin{aligned}
\langle q \rangle_c &= \langle q \rangle\,, \\
\langle q^2 \rangle_c &= \langle q^2 \rangle - \langle q \rangle^2\,, \\
\langle q^3 \rangle_c &= \langle q^3 \rangle - 3\langle q \rangle \langle q^2 \rangle + 2\langle q \rangle^3\,, \\
\langle q^4 \rangle_c &= \langle q^4 \rangle - 4\langle q^3 \rangle \langle q \rangle - 3\langle q^2 \rangle^2 + 12\langle q^2 \rangle \langle q \rangle^2 - 6\langle q \rangle^4\,.
\end{aligned}$$

Figure 2 shows the second order cumulant $\langle q^2 \rangle_c$ as a function of temperature for various double-well potentials, $c = 0$ (a), $c = 1$ (b), $c = 2$ (c), $c = 4$ (d). The classical approximation gives good result at high temperature ($T > 600\,\text{K}$ for $c = 0$ (a), $T > 200\,\text{K}$ for $c = 1$ (b), $T > 300\,\text{K}$ for $c = 2$ (c), $T > 500\,\text{K}$ for $c = 4$ (d)). At low temperature, the classical probability density has a sharp peak and the classical approximation gets poor. In particular, for a symmetric potential ($c = 0$) the classical approximation gives two sharp peak at ± 0.1 Å in the probability density at $T \sim 0\,\text{K}$. Thus the classical second order cumulant $\langle q^2 \rangle_c$ approaches to $0.01\,\text{Å}^2$ and gives the largest difference from the quantum result. The zero point vibration energy depends on the ω (as $E = \frac{1}{2}\,\hbar\omega$) and the relation between ω and the second order curvature at the bottom of deeper potential well is $\omega \propto 1/v''(q_{\min})$. The quantum second order cumulant $\langle q^2 \rangle_c$ means zero point vibration at 0 K. It is expected that the larger the curvature $v''(q_{\min})$, the smaller the second order

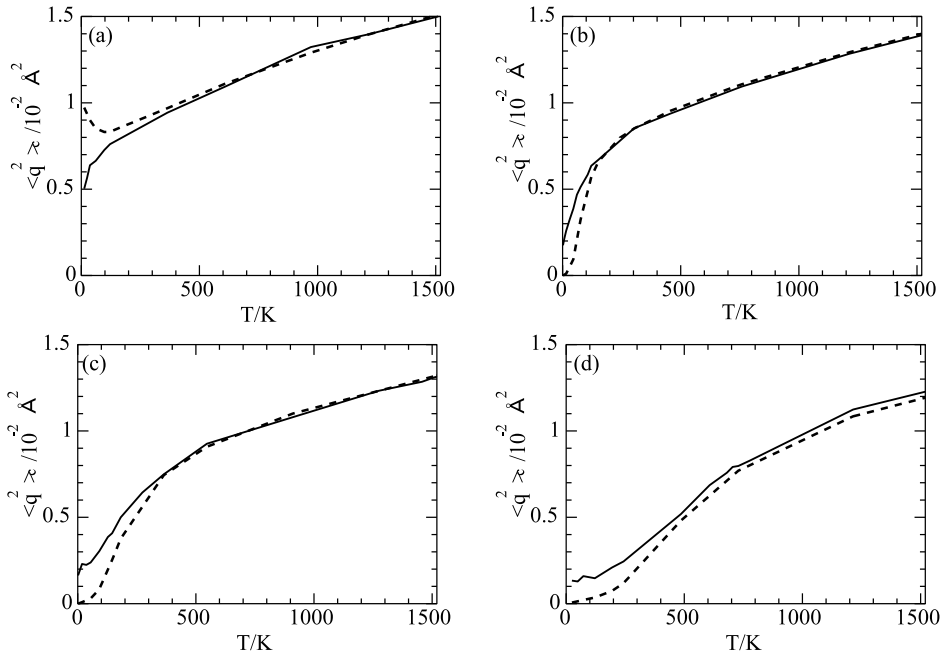

Fig. 2. The temperature dependence of the quantum and classical second order cumulant $\langle q^2 \rangle_c$ for four different double-well potentials; (a) $c = 0$, (b) $c = 1$, (c) $c = 2$, (d) $c = 4$.

cumulant $\langle q^2 \rangle_c$. The value of $\langle q^2 \rangle_c$ at $T = 1.52\,\mathrm{K}$ (this is an example for low temperature) is the smallest in the case that $c = 4(\langle q^2 \rangle_c \approx 0.00134\,\mathrm{\AA}^2)$, which increases as the c value decreases, because higher potential well at $q = -0.1\,\mathrm{\AA}$ becomes flat due to tunneling probability.

Figure 3 shows the third order cumulants $\langle q^3 \rangle_c$ as functions of temperature for three different double-well potentials $c = 1$ (a), $c = 2$ (b), $c = 4$ (c). In the case of the symmetric double-well potential ($c = 0$), both quantum and classical third order cumulants vanish, $\langle q^3 \rangle_c = 0$ irrespective of temperature, because both the classical potential and quantum local effective potential $V_L(q)$ is symmetric: The third order cumulant $\langle q^3 \rangle_c$ reflects asymmetry of the potential. In the case of $c = 1$ and $c = 2$, $\langle q^3 \rangle_c$ shows minimum ($|\langle q^3 \rangle_c|$ is the largest) indicated by arrows at $\sim 100\,\mathrm{K}$ ($c = 1$) and $\sim 550\,\mathrm{K}$ ($c = 2$) in the quantum calculations. In higher temperature region, the quantum local effective potential is reduced to the bare potential $V(q)$, so $\langle q^3 \rangle_c$ shows the same behavior at high temperature. We should note that quantum and classical third order cumulants $\langle q^3 \rangle_c$ are nearly the same for $c = 4$, because the quantum tunneling probability is expected to be quite small. This characteristic temperature at minimum of the third order cumulant shifts to higher when c increases. If we observe the minimum in temperature dependence of the third-order cumulant for certain atomic pair, it shows that the double-well

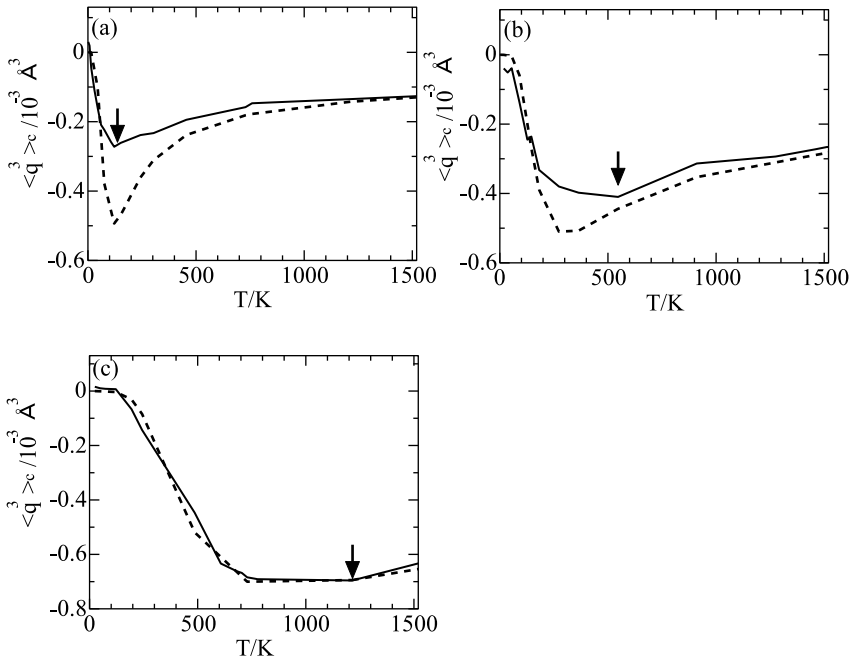

Fig. 3. The temperature dependence of the quantum (solid line) and classical (dashed line) third order cumulant $\langle q^3 \rangle_c$ for three different double-well potential; (a) $c = 1$, (b) $c = 2$, (c) $c = 4$. The arrows indicate the minimum points, T_m.

potential is asymmetrical and we can estimate the potential shape (or c-value) of the potential from that minimum temperature. Similar phenomenon is observed in the fourth order cumulant $\langle q^4 \rangle_c$ (in this case, maximmum point) discussed later.

3.2 EXAFS thermal damping function

In this section, we discuss EXAFS thermal damping function $G(k)$ defined by [13]

$$G(k) = \big\langle \exp(2\mathrm{i}kq) \big\rangle = \int_{-\infty}^{\infty} \exp(2\mathrm{i}kq) P(q) \mathrm{d}q \,. \tag{14}$$

This function can be written in the cumulant expansion as far as that expansion converges. Actually it rapidly converges in weak anharmonic systems;

$$\begin{aligned} G(k) = \exp\big\{ -2k^2 \langle q^2 \rangle_c + \tfrac{2}{3}\, k^4 \langle q^4 \rangle_c - \ldots \big\} \\ \times \exp\big\{ \mathrm{i}\big(k \langle q \rangle_c - \tfrac{4}{3}\, k^3 \langle q^3 \rangle_c + \ldots \big) \big\} \,. \end{aligned} \tag{15}$$

Equation (14) can be applied to any strongly anharmonic systems, whereas eq. (15) can be only applied to weak anharmonic systems. Now we separately calculate

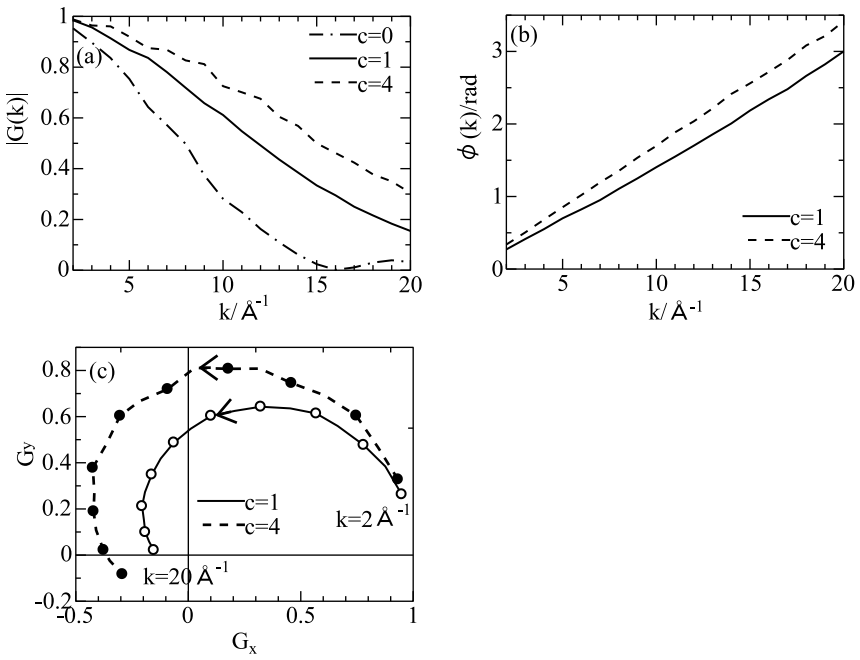

Fig. 4. The amplitude $|G(k)|$ (a), the phase $\phi(k)$ (b), and complex plane expression (G_x, G_y) (c) in the thermal damping function $G(k)$ of EXAFS at temperature 15.2 K for three different potentials. The black and white dots is plotted at 2 Å^{-1} intervals.

$|G(k)|$ and phase $\phi(k)$

$$|G(k)| = \sqrt{\left(\int_{-\infty}^{\infty} \cos(2kq)P(q)\mathrm{d}q\right)^2 + \left(\int_{-\infty}^{\infty} \sin(2kq)P(q)\mathrm{d}q\right)^2}$$
$$\approx \exp\left\{-2k^2\langle q^2\rangle_c + \tfrac{2}{3}\,k^4\langle q^4\rangle_c - \ldots\right\}, \tag{16}$$
$$\phi(k) = \tan^{-1}\left(\frac{\int_{-\infty}^{\infty} \sin(2kq)P(q)\mathrm{d}q}{\int_{-\infty}^{\infty} \cos(2kq)P(q)\mathrm{d}q}\right) \approx k\langle q\rangle_c - \frac{4}{3}\,k^3\langle q^3\rangle_c \ldots . \tag{17}$$

We also use another form to study specific features in $|G(k)|$ and $\phi(k)$ from different point of view,

$$(G_x, G_y) = (\mathrm{Re}\, G, \mathrm{Im}\, G)\,. \tag{18}$$

The strength $|G(k)|$ dominates the envelop of EXAFS oscillation function $\chi(k)$, and the phase $\phi(k)$ appears in sinusoidal function of $\chi(k)$. The trajectories of (G_x, G_y) on the complex plane contains useful information on the thermal factor $G(k)$.

Figures 4 and 5 show the amplitude (a) $|G(k)|$, (b) the phase $\phi(k)$, and (c) (G_x, G_y) on the complex plane for three potentials $T = 15.2\,\mathrm{K}$ (Fig. 4), 1520 K (Fig. 5). For symmetric potential $c = 0$, $G(k)$ has to be real and the point (G_x, G_y)

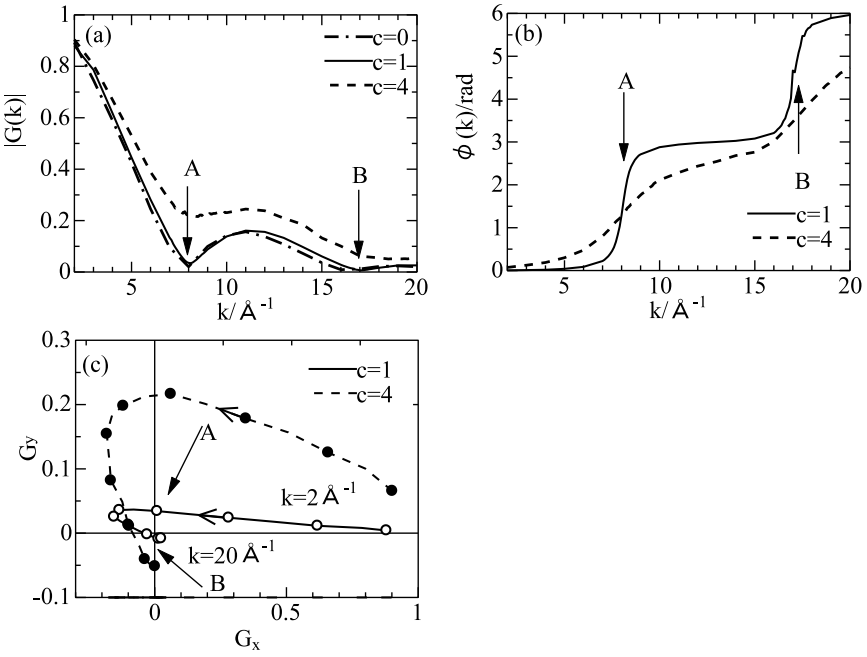

Fig. 5. The amplitude $|G(k)|$ (a), the phase $\phi(k)$ (b), and complex plane expression (G_x, G_y) (c) in thermal damping function $G(k)$ of EXAFS at temperature 1520 K for three different potentials. The arrows A and B are the position where the "beat" is observed. The black and white dots is plotted at 2 Å^{-1} intervals.

in the complex plane oscillates just on real axes which is not plotted here. At low temperature $T = 15.2$ K (Fig. 4), as c increases, $|G(k)|$ weakly dumps because of the small tunneling probability. The phase $\phi(k)$ for both $c = 1$ and 4 show monotonically increasing function of k. In the complex plane, the trajectry for $c = 4$ is far from real axis in comparison with that for $c = 1$ for asymmetric potential. If potential is symmetric, the trajectory is close to real axis. This means that the trajectory on complex plane can be an indicator of the asymmetricity of the atomic pair potential.

At high temperature $T = 1520$ K (Fig. 5), the amplitude $|G(k)|$ shows "beat" for $c = 0$, 1 and 4 at 8 Å^{-1} (arrow A in Fig. 5). The beat can be related to the small difference in the atomic distances [25]

$$2k\Delta r = (2n+1)\pi\,, \quad n = 0, 1, 2, \ldots\,, \tag{19}$$

where Δr is the small difference in the interatomic distances. In the present double-well system $\Delta r = 0.2$ Å, so that the beat is expected at $k \cong 8.0$ Å^{-1}, which is consistent with our result at 1520 K, where the quantum tunneling effect can be neglected. We also observe the beat for $c = 4$ but it is not so pronounced. The phase for $c = 1$ shows steps at 8 Å^{-1} (arrow A) and 17 Å^{-1} (arrow B), where the

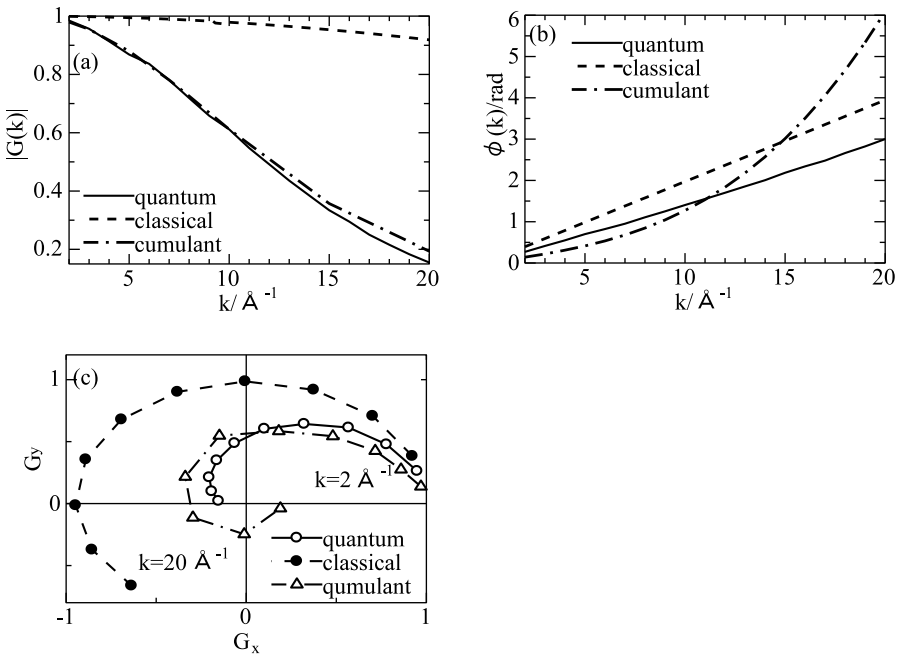

Fig. 6. The intensity $|G(k)|$ (a) and phase $\phi(k)$ (b) and complex plane expression (c) of thermal EXAFS damping function $G(k)$ for the quantum (solid line) and the classical (dashed line) approaches at $T = 15.2\,\mathrm{K}$. The cumulant expansion up to fourth order (dash–dotted line) is also presented.

jump is about π. The beat is more remarkable at high temperature than at low temperature. In Fig. 5(c), we plot (G_x, G_y) near the real axis for $c = 1$; because $P(q)$ is a symmetric function, we see that $G_y \neq 0$. The phase of $G(k)$ rapidly changes near at $8\,\mathrm{Å}^{-1}$ (arrow A) and $17\,\mathrm{Å}^{-1}$ (arrow B) where the beat is observed. The characteristic feature in Fig. 5 (a) and (b) are understood from the trajectory of (G_x, G_y) for the quantum calculation. From $2\,\mathrm{Å}^{-1}$ to $10\,\mathrm{Å}^{-1}$ it is nearly on the straight line which • crosses the imaginary axis at $8\,\mathrm{Å}^{-1}$ almost parallel to the real axis. So that we find $|G(k)|_{\mathrm{min}}$ at $\sim 8\,\mathrm{Å}^{-1}$. From $12\,\mathrm{Å}^{-1}$ to $20\,\mathrm{Å}^{-1}$ the trajectory is again on a straight line quite close to the origin, which gives small $|G(k)|$ as observed in Fig. 5 (a) wheras gives large change in $\phi(k)$ (see Fig. 5 (b)).

Next, we discuss the validity of the classical approximation and the cumulant expansion of the damping function $G(k)$. Figure 6 shows (a) the amplitude $|G(k)|$, (b) phase $\phi(k)$ and (c) complex plane expression of the thermal damping function for the quantum path-integral (solid line) and the classical (dashed line) calculations at $T = 15.2\,\mathrm{K}$ for $c = 1$. The cumulant expansion up to fourth order (dash–dotted line) is also shown. As the classical approximation is poor at low temperature, the amplitude $|G(k)|$ in the classical approximation really gives a poor agreement with the quantum path-integral calculation because the probability density $P(q)$ is

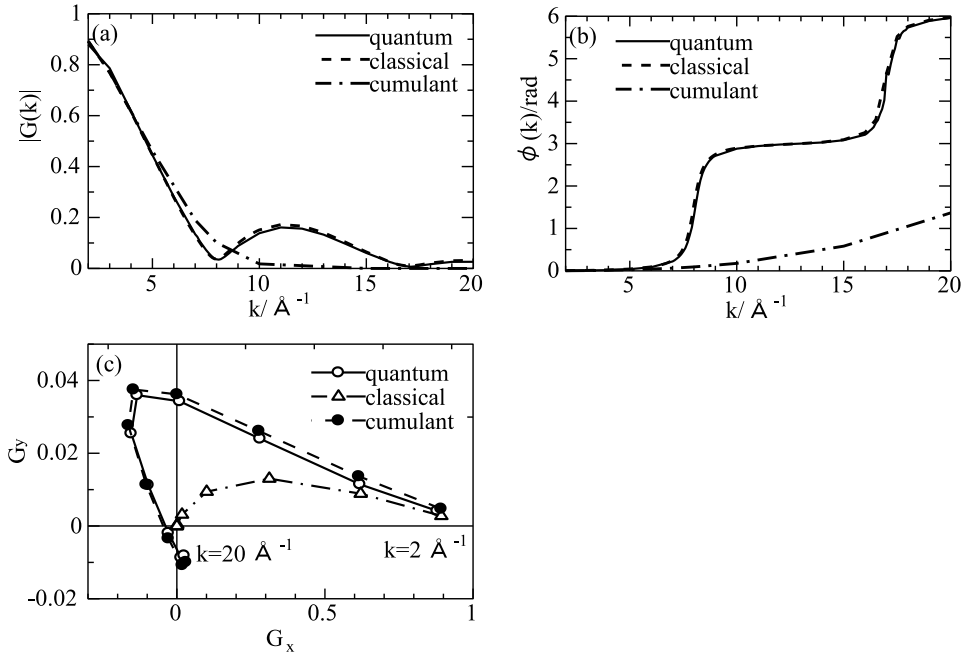

Fig. 7. The amplitude $|G(k)|$ (a) and phase $\phi(k)$ (b) and complex plane expression (c) in thermal damping function $G(k)$ of EXAFS for the quantum (solid line) and the classical (dashed line) calculations at $T = 1520\,\mathrm{K}$. The cumulant expansion up to fourth order (dotted line) is also shown.

strongly affected by tunneling. On the other hands, the cumulant expansion gives good agreement with the quantum path-integral calculation. The quantum path-integral calculation for the phase $\phi(k)$ monotonically increases, and the classical result is similar to the quantum result, but is a little larger. On the other hand, the cumulant expansion is quite good up to $k = 12\,\mathrm{Å}^{-1}$, whereas gets a little poor above $12\,\mathrm{Å}^{-1}$. In the complex plane expression (c), the trajectory for the classical approximation is similarly expanded from the trajectory for the quantum path-integral approach. This is reason why they show similar behavior in $\phi(k)$ but different behavior in $|G(k)|$. The trajectory for the cumulant approximation is quite close to the quantum trajectory, which gives rise to the nearly same $|G(k)|$, whereas $G(k)$ moves more rapidly for the cumulant approximation, in particular at large k, than for the quantum method which results in the large difference of $\phi(k)$. In contrast to the quantum calculation, the classical calculation gives a trajectory whose part from $7\,\mathrm{Å}^{-1}$ to $10\,\mathrm{Å}^{-1}$ • is nearly on a circle around the origin: This gives $|G(k)| \sim$const. in that region.

Figure 7 shows (a) the amplitude $|G(k)|$, (b) phase $\phi(k)$ and (c) complex plane expression in the thermal damping function of EXAFS for the quantum path-integral (solid line) and the classical (dashed line) calculation at $T = 1520\,\mathrm{K}$ for

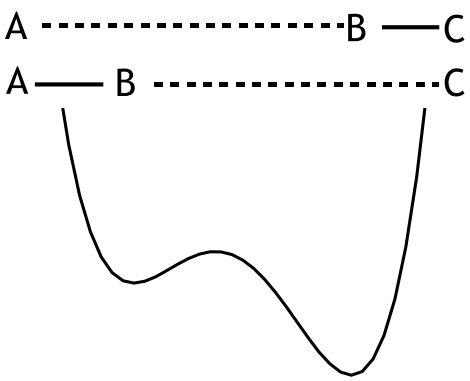

Fig. 8. The schematic model double-well potentials for the chemical reaction expressed by eq. (20)

$c = 1$. The cumulant expansion up to fourth order (dotted line) is also shown. At such high temperature, the bare potential and the local effective potential is almost the same and the classical approximation gives a good result in $|G(k)|$, and $\phi(k)$. The cumulant expansion up to fourth order cannot predict the observed "beat".

3.3 Application to chemical reaction rate

In this subsection we apply the path integral effective potential method to study quantum tunneling effects in chemical reaction process. Figure 8 shows schematically the double-well potential for a chemical reaction, where the reaction is assumed as

$$\mathrm{A}\cdots\mathrm{B}-\mathrm{C} \xrightarrow{k_1} \mathrm{A}-\mathrm{B}\cdots\mathrm{C}\,, \tag{20}$$

where k_1 is the reaction rate constant for this reaction. We assumed that B atom moves in the double-well potential, whereas A and C atoms are fixed at the left and right hand sides of the potential (see Fig. 8). A chemical bond B–C is formed when the atom B is in the right well of the potential. On the other hand, the bond A-B formed if the atom B moves to the left well. Figure 9 shows model potentials used for the present calculations with same potential barrier at $q = 0$ for various c-values (g-values are adjusted). We assume that k_1 is expressed equation as,

$$k_1 = C \exp\left(-\frac{E_a}{k_{\mathrm{B}}T}\right), \tag{21}$$

where C is a frequency constant and E_a is an activation energy of the reaction which is equivalent to the potential barrier from the lower well ($q = 0.1$ Å). Figure 10 shows the Arrhenius plot of $\log k_1$ as a function of $1/T$. We calculate these values of $\log k_1$ vs. $1/T$, where the activation energy E_a is replaced by the effective potential barrier of the local effective potential expressed by eq.(7) as same manner as described in ref. [21]. Therefore these plots contain the quantum tunneling

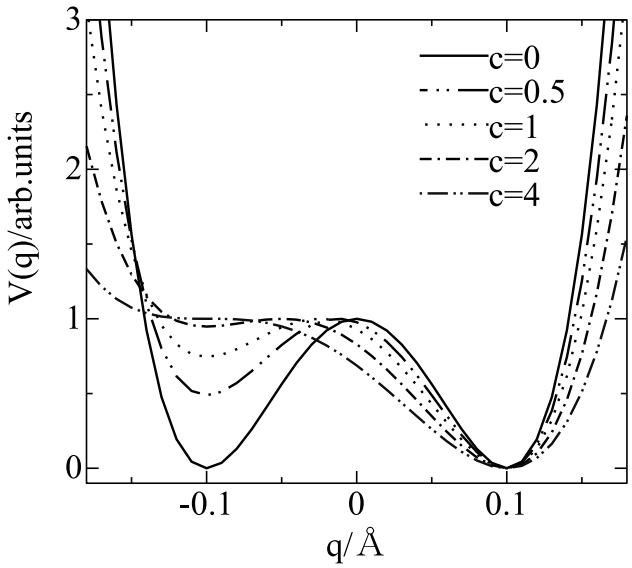

Fig. 9. The model double-well potentials for the chemical reaction coordinate for $c = 0$ ($g = 1.74$), $c = 0.5$ ($g = 2.15$), $c = 1$ ($g = 2.61$), $c = 2$ ($g = 3.38$), $c = 4$ ($g = 5.69$). The barrier is kept constant for various c-values.

effect in the chemical reaction shown by eq.(20). Dotted straight line shows the classical limit where the effective potential is same as bare potential. That is, E_a is the potential barrier and it does not depend on c-values. Other curves deviated from the classical straight line show the tunneling behaviors. The tunneling effect is stronger for smaller c-value (more symmetric potential). We should note that the tunneling effect is different even for the same potential barrier (or E_a). The tunneling probability is quite sensitive to the hight of the potential well of the chemical product side. It is another interesting point that the result of $c = 4$ (strongly asymmetric single-well potential) is quite close to that in case of Morse type potential discussed previously [21].

The present result shown in Fig. 10 can be considered as the model for the reaction as

$$(p-)\mathrm{H}_2 + \mathrm{H} \rightarrow \mathrm{H} + (o-)\mathrm{H}_2\,, \tag{22}$$

where atoms A, B and C are replaced as H (hydrogen) atoms [26]. In the previous study [26] experimental result was compared to the theoretical result calculated using the Eckart potential as the tunneling model. The present path integral results reproduce such a behavior well.

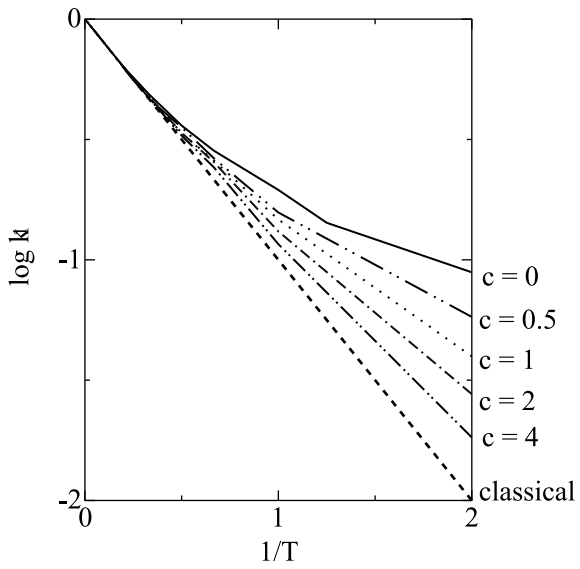

Fig. 10. The Arrhenius plot for the model double-well potentials for $c = 0$ ($g = 1.74$), $c = 0.5$ ($g = 2.15$), $c = 1$ ($g = 2.61$), $c = 2$ ($g = 3.38$), $c = 2$ ($g = 5.69$). The dashed straight line is classical result.

4 Conclusion

The real space method based on finite temperature path integral theory has been applied to the EXAFS thermal factors for strongly anharmonic systems. The path integral calculation shows quite different distribution function $P(q)$ from the classical one, in particular, for $c = 0$, (the symmetric double-well potential). It has a peak at $q = 0$ Å because of tunneling effect through the potential barrier. The asymmetric potentials give rise to peak shift from the potential bottom.

The two characteristic features are observed for the asymmetric double well potential:

(1) The amplitude of EXAFS damping function $|G(k)|$ shows "beat" in the case of the double-well potential. We can estimate the distance between the two bottoms of potential from the wave number at the "beat".

(2) In the temperature dependence of third (fourth) order cumulants, there is minimum (maximum) point (T_m) which is characteristic for the double-well potential and reflects the asymmetric potential shape.

The asymmetric double-well potential is applied to chemical reaction coordinate for the simple unimolecule reaction system. The path integral effective potential method well reproduces the behavior of the quantum tunneling effect.

References

[1] G. Beni and P.M. Platzman: Phys. Rev. B **14** (1976) 1514.

[2] J.M. Tranquada and R. Ingalls: Phys. Rev. B **28** (1983) 3520.

[3] T. Fujikawa and T. Miyanaga: J. Phys. Soc. Jpn. **62** (1993) 4108.

[4] T. Miyanaga and T. Fujikawa: J. Phys. Soc. Jpn. **63** (1994) 1036

[5] T. Miyanaga and T. Fujikawa: J.Phys. Soc. Jpn. **63** (1994) 3683.

[6] T. Fujikawa, M. Yimagawa and T. Miyanaga: J. Phys. Soc. Jpn. **64** (1995) 2047.

[7] P. Rennert: Jpn. J. Appl. Phys. S **32-2** (1993) 19.

[8] A.I. Frenkel and J.J. Rehr: Phys. Rev. B **48** (1993) 585.

[9] T. Yokoyama, T. Satsukawa and T. Ohta: Jpn. J. Appl. Phys. **28** (1989) 1905.

[10] R.P. Feynman: in *Statistical Mechanics*. Benjamin, Reading, Massachusetts, 1972.

[11] A. Cuccoli, R. Giachetti, V. Tognetti, R. Vaia and P. Verrucchi: J. Phys. Condens, Matter. **7** (1995) 7891.

[12] R.P. Feynman and H. Kleinert: Phys. Rev. B **33** (1986) 7647.

[13] T. Fujikawa, T. Miyanaga and T. Suzuki: J. Phys. Soc. Jpn. **66** (1997) 2897.

[14] T. Miyanaga and T. Fujikawa: J. Phys. Soc. Jpn. **67** (1998) 2930.

[15] T. Miyanaga, T. Suzuki and T. Fujikawa: J. Synchrotron Rad. **7** (2000) 95.

[16] T. Yokoyama: Phys. Rev. B **57**(1998) 3423.

[17] S. a Beccara, G. Dalba, P. Fornasini, R Grisentini, F. Pederiva and A. Sanson: Phys. Rev. B **68** (2003) 1403.

[18] D.L. Freeman and J.D. Doll: Annu. Rev. Phys. Chem. **47** (1996) 43.

[19] T. Goto, Y. Nemoto, K. Sakai, T. Yamaguchi, M. Akatsu, T. Yanagisawa, H. Hazama and K. Onuki: Phys. Rev. B **69** (2004) 180511.

[20] J.I. Steinfeld, J.S. Francisco and W.L. Hase: in *Chemical Kinetics and Dynamics*. Prentice-Hall, 1989.

[21] T. Miyanaga and T. Fujikawa: Chem. Phys. Letters **308** (1999) 78.

[22] J.D. Doll: J. Chem. Phys. **81** (1984) 3536.

[23] J. Mustre de Leon, S.D. Conradson, I. Bastic, A.R. Bishop, I.D. Raistrick, M.C. Aronson and F.H. Garzon: Phys. Rev. B **45** (1992) 2447.

[24] E.D. Crozier, N. Alberding, K.R. Bauchspiess, A.J. Seary and S. Gygax: Phys. Rev. B **36** (1987) 8288.

[25] E.D. Crozier: Physica B **158** (1989) 14.

[26] W.R. Schulz and D.J. LeRoy: J. Chem. Phys. **42** (1965) 3869.